

Hydraulic jumps in a channel

DANIEL BONN¹, ANDERS ANDERSEN²†
AND TOMAS BOHR²

¹van der Waals-Zeeman Institute, Valckenierstraat 65, 1018 XE Amsterdam, The Netherlands

²Department of Physics and Center for Fluid Dynamics, Technical University of Denmark,
DK-2800 Kgs. Lyngby, Denmark

(Received 26 March 2008 and in revised form 1 August 2008)

We present a study of hydraulic jumps with flow predominantly in one direction, created either by confining the flow to a narrow channel with parallel walls or by providing an inflow in the form of a narrow sheet. In the channel flow, we find a linear height profile upstream of the jump as expected for a supercritical one-dimensional boundary layer flow, but we find that the surface slope is up to an order of magnitude larger than expected and independent of flow rate. We explain this as an effect of turbulent fluctuations creating an enhanced eddy viscosity, and we model the results in terms of Prandtl's mixing-length theory with a mixing length that is proportional to the height of the fluid layer. Using averaged boundary-layer equations, taking into account the friction with the channel walls and the eddy viscosity, the flow both upstream and downstream of the jump can be understood. For the downstream subcritical flow, we assume that the critical height is attained close to the channel outlet. We use mass and momentum conservation to determine the position of the jump and obtain an estimate which is in rough agreement with our experiment. We show that the averaging method with a varying velocity profile allows for computation of the flow-structure through the jump and predicts a separation vortex behind the jump, something which is not clearly seen experimentally, probably owing to turbulence. In the sheet flow, we find that the jump has the shape of a rhombus with sharply defined oblique shocks. The experiment shows that the variation of the opening angle of the rhombus with flow rate is determined by the condition that the normal velocity at the jump is constant.

1. Introduction

The hydraulic jump is what appears in a kitchen sink when opening the water tap: the water jet impacts the sink, the jet spreads radially in a shallow fluid layer, and after some distance the layer thickens abruptly and forms a circular jump (Rayleigh 1914; Tani 1949; Watson 1964; Olsson & Turkdogan 1966). Most recent studies of hydraulic jumps are concerned with circular jumps (Higuera 1994; Hornung, Willert & Turner 1995; Svendsen *et al.* 2000; Holland *et al.* 2002; Defina & Susin 2003).

The hydraulic jump was originally explained by Rayleigh (1914) as a shock. At the jump, the flow speed, v , decreases abruptly from 'supersonic' to 'subsonic' with respect to the local surface wave speed. In a shallow layer of height h , the speed of gravity waves is given by $\sqrt{g_0 h}$, where g_0 is the acceleration due to gravity. The

† Email address for correspondence: aanders@fysik.dtu.dk

corresponding dimensionless number is the Froude number, $Fr = v/\sqrt{g_0 h}$. The flow upstream of the jump, being more rapid than the surface waves, is referred to as supercritical with $Fr > 1$, while the flow downstream of the jump is referred to as subcritical with $Fr < 1$. The supercritical flow depends only on upstream conditions, whereas the subcritical flow depends on both upstream and downstream conditions. In shallow layers, the hydraulic jump is usually connected with separation (Tani 1949; Bohr, Dimon & Putkaradze 1993) and thus viscous friction is essential. For the circular jump, mass conservation naturally leads to a decrease of the height of the supercritical fluid layer and thus to large viscous stresses. The one-dimensional case is different: we observe experimentally that the flow upstream of the jump has a linearly increasing height profile, but that it still leads to an abrupt hydraulic jump (Watson 1964; Bohr, Putkaradze & Watanabe 1997; Ruschak, Weinstein & Ng 2001; Watanabe, Putkaradze & Bohr 2003; Singha, Bhattacharjee & Ray 2005). In rivers, where viscous effects are less important, stationary hydraulic jumps occur only because of inhomogeneities in the river bed, whereas the so-called river bores are travelling jumps with a complicated wave structure (Chow 1959; Simpson 1997).

In this paper, we analyse quasi one-dimensional hydraulic jumps under steady flow conditions. We do this both for flows in narrow channels and flows in a wide sheet. In the narrow channels the influence of the inlet and the channel walls leads to turbulence even at moderate Reynolds numbers. We argue that this is the reason for the strongly enhanced slope of the supercritical height profile, which turns out to be independent of flow rate. We model this by introducing an eddy viscosity derived from a mixing length proportional to the local height of the fluid layer. The position of the jump is determined by the boundary conditions at the channel inlet and outlet, and not necessarily by a local instability of the flow. In the sheet case, the hydraulic jump emerges at the edges of the sheet and creates a triangular oblique shock. The variation of the opening angle with flow rate shows that the normal velocity is approximately independent of flow rate.

2. Experimental methods

2.1. Channel experiment

We formed a stationary hydraulic jump in a channel with a horizontal bottom by confining a water jet between two parallel vertical walls. The walls and the bottom of the channel were made of polymethylmethacrylate (PMMA). Water on PMMA has a contact angle of approximately 90° , and effects of wetting films on the walls were therefore negligible. The channel width was 0.4 cm, 0.8 cm and 1.2 cm, respectively, in three different experimental set-ups, and the total channel length was 100 cm in all three experiments. The channel ends abruptly, and the fluid flows freely out of the channel over the vertical end faces. Water was pumped at constant flow rate, measured using a flow-meter, into the channel through a nozzle placed a few millimetres above the channel bottom, as shown in the sketch of the central part of the channel in figure 1. The rectangular nozzle filled the entire width of the channel, and the nozzle was placed at the midpoint of the channel. Water exited the nozzle symmetrically toward both left and right, thereby forming hydraulic jumps both to the left and to the right of the nozzle. We used the left–right symmetry of the flow to check the precise alignment of the nozzle and the channel. We measured the height of the fluid layer using either a depth micrometre mounted vertically above the water surface or by identifying the surface and the channel bottom in high-resolution digital photographs taken through the transparent channel walls. The dotted curves in figure 2 show the

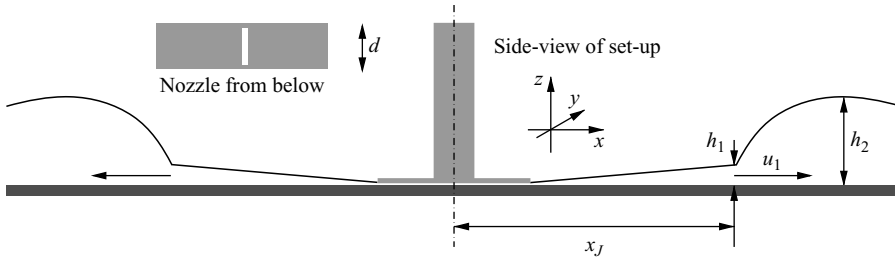


FIGURE 1. Schematic illustration of the experimental apparatus for the channel flow. We use x to denote the lengthwise direction, y for the lateral direction, and z for the vertical direction.

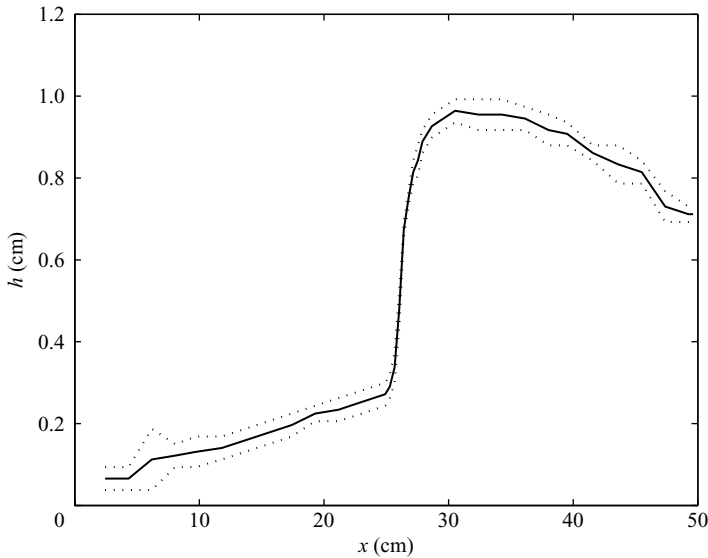


FIGURE 2. Measured height profile for the hydraulic jump in the 0.8 cm channel with the flow rate per unit transverse length $q = 10.0 \text{ cm}^2 \text{ s}^{-1}$. The dotted curves show the upper and the lower surface height, and the solid curve shows the average of the two dotted curves.

surface height at the channel walls and in the middle of the channel identified in the digital photographs of the hydraulic jump in the 0.8 cm channel with the flow rate per unit transverse length $q = 10.0 \text{ cm}^2 \text{ s}^{-1}$. The surface profile in figure 2 is a representative example of the measured height profiles in the three channels. We use the average surface height in the following analysis.

2.2. Sheet experiment

A second experiment was carried out with the focus on the jump condition for the one-dimensional hydraulic jump. For this, instead of a jet, a thin sheet of water was made to impact a horizontal plate (figure 3). Again, water was used, and the flow rate was held constant and measured with a flow-meter. For quantitative measurements, a set-up was used in which the sheet emanated from a $3.0 \text{ cm} \times 0.1 \text{ cm}$ orifice made of PMMA. Since the lateral extension of the sheet (3.0 cm) was much larger than its width (0.1 cm) the film expanded only in one direction. The orifice was positioned a few millimetres above the PMMA plate on which the sheet impacted, allowing for a direct visualization of the hydraulic jump from below through the transparent plate.

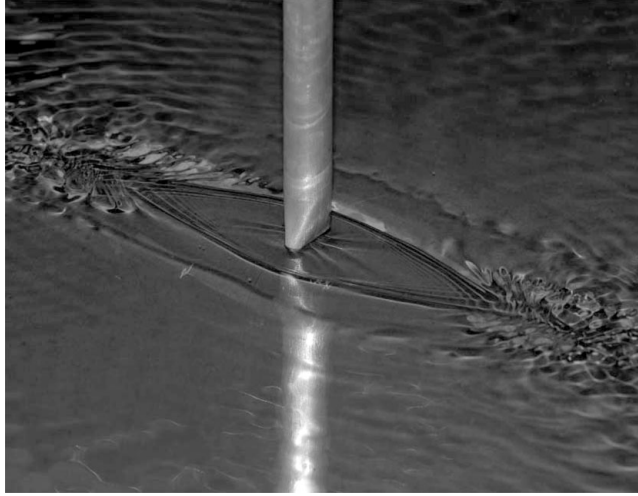


FIGURE 3. Hydraulic jump with the shape of a rhombus formed by a sheet of water emerging from a slit and impacting on a flat and horizontal plate. Two different experimental set-ups were used. The first set-up which is shown in the figure gave a particularly clear demonstration of the effect, but it did not allow for good quantitative measurements since the sheet thickness was fluctuating. A second set-up was therefore machined in PMMA to give a $3.0\text{ cm} \times 0.1\text{ cm}$ sheet and allow for measurements of the opening angle as a function of the flow rate.

The height of the fluid layer was measured with a depth micrometre attached to a translation table whose displacement could be read off to an accuracy of $1/100\text{ mm}$.

3. Height profiles in the channel experiment

3.1. Height profiles before the jump

Figure 4 shows the height of the fluid layer, h , as a function of the horizontal distance from the nozzle centre, x , for different flow rates per unit transverse length, q , in the channel experiment with wall separation $d = 0.8\text{ cm}$. For the channels with $d = 0.4\text{ cm}$ and $d = 1.2\text{ cm}$, we measured qualitatively similar profiles. The position of the abrupt hydraulic jump x_J is displaced downstream when q is increased, and with the largest value of q (black) we do not observe a jump in the channel. The most obvious and surprising feature of the flow is that the height of the supercritical flow upstream of the jump increases linearly with x from the nozzle to the jump position. This can be understood easily by noting that the flow is predominantly horizontal and strongly sheared in the vertical direction. The important terms in the Navier–Stokes equation are therefore

$$u \frac{\partial u}{\partial x} = \nu \frac{\partial^2 u}{\partial z^2}, \quad (3.1)$$

where u is the velocity in the x -direction, ν is the kinematic viscosity of the fluid, and where we have neglected the hydrostatic pressure and used $h \ll d$. Using mass conservation, which in terms of the average velocity $v = \langle u \rangle$ can be written $q = hv$, we find the following estimate of the slope of the surface height

$$-\frac{q^2}{h^3} \frac{dh}{dx} \sim -\nu \frac{q}{h^3} \quad \text{or} \quad \frac{dh}{dx} \sim \frac{\nu}{q}. \quad (3.2)$$

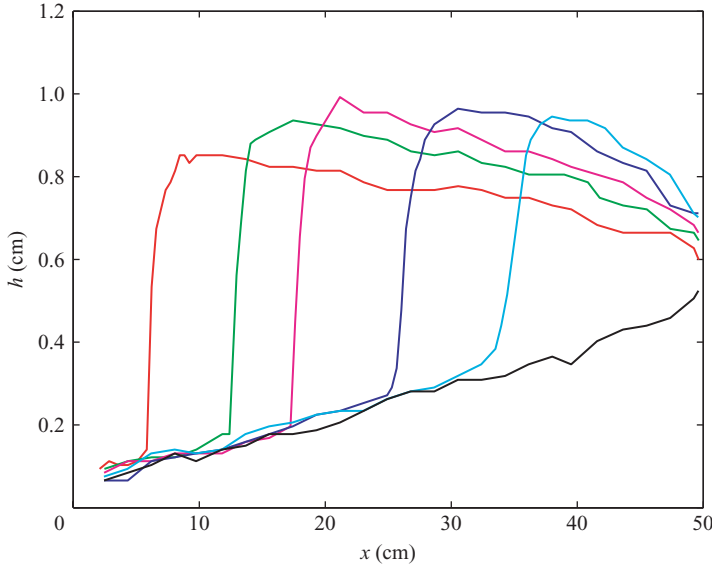


FIGURE 4. Measured height profiles for hydraulic jumps in the 0.8 cm channel. The flow rate per unit transverse length was $q = 4.6 \text{ cm}^2 \text{ s}^{-1}$ (red), $q = 6.5 \text{ cm}^2 \text{ s}^{-1}$ (green), $q = 7.8 \text{ cm}^2 \text{ s}^{-1}$ (magenta), $q = 10.0 \text{ cm}^2 \text{ s}^{-1}$ (blue), $q = 11.6 \text{ cm}^2 \text{ s}^{-1}$ (cyan) and $q = 17.2 \text{ cm}^2 \text{ s}^{-1}$ (black).

This result was shown by Watson (1964) to follow from the boundary-layer equations in the one-dimensional case. Assuming gravity to be negligible, which is reasonable for the supercritical flow, we find a self-similar velocity profile

$$u(x, z) = v(x)f(z/h(x)), \quad (3.3)$$

and the linearly increasing free surface height

$$h(x) = \frac{\pi v}{\sqrt{3}q}(x - x_0) \approx 1.81 \frac{v}{q}(x - x_0). \quad (3.4)$$

The slopes of the measured height profiles are up to an order of magnitude larger than those predicted by the laminar theory as shown by the dashed line in figure 5 in a representative case. Furthermore, the inverse proportionality of the slope with the flow rate in (3.4) is not observed in the experiments, and within the experimental accuracy, we find that the slope is independent of flow rate as figure 4 shows.

3.2. Mixing-length model

We suggest the following interpretation of the observed height profiles: the appearance of a turbulent eddy viscosity. The Reynolds number for a channel flow with characteristic velocity v and length scale h is $Re = hv/v = q/v$. Here we have chosen the height h as the characteristic length scale, since h is the smallest length scale in the supercritical regime and significantly smaller than the channel width d . Note that Re is independent of x with this definition. In the present experiment, $Re \approx 10^3$. More precisely, for the flows shown in figure 4 from the 0.8 cm channel, we have $460 \leq Re \leq 1720$. Although these Reynolds numbers are not very large, turbulence occurs owing to the strong mixing created by reflections from the sidewalls and, indeed, adding particles that visualize the flow field, shows irregular motion indicative

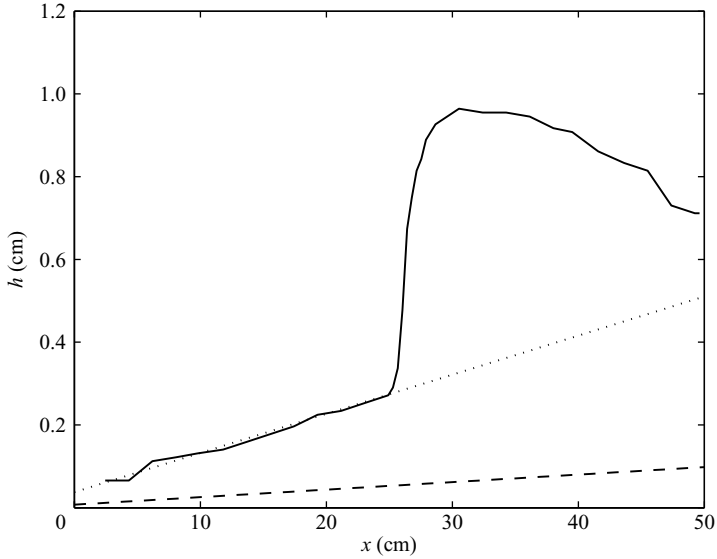


FIGURE 5. Measured height profile (solid curve) for the flow in the 0.8 cm channel with $q = 10.0 \text{ cm}^2 \text{ s}^{-1}$. The dashed line shows the prediction of the laminar model (3.4) and the dotted line the result of the mixing length model of the eddy viscosity (3.5) with $\kappa = 0.07$.

of turbulence (figure 6). In the simplest model, the mixing-length theory of Prandtl (Pope 2000; White 2006), turbulence is modelled in the spirit of kinetic theory as causing fluid particles to make random jumps transverse to the flow and thus enhancing momentum transfer. Assuming that the typical jump has a size l_m – the mixing length – we find an enhanced eddy viscosity ν_ε which is proportional to l_m multiplied by the typical velocity fluctuation $\Delta u \approx l_m \partial u / \partial z$, where z is the vertical coordinate, transverse to the flow and where $\partial u / \partial z$ is the shear rate of the mean flow. Thus, $\nu_\varepsilon \approx (l_m)^2 |\partial u / \partial z|$. The crucial assumption is now that the mixing length must be proportional to the height of the fluid layer. This is reasonable as long as h is the smallest length scale, which is true in the supercritical region. In turbulent boundary layers, a standard choice is similarly a mixing length proportional to the boundary-layer thickness, δ , as discussed by White (2006). Letting $l_m = \kappa h$, we can now estimate the eddy viscosity:

$$\nu_\varepsilon \approx \kappa^2 q. \quad (3.5)$$

Thus, ν_ε is proportional to q , and when replacing ν with ν_ε in (3.4) we therefore obtain a linear height profile with a slope that is independent of q . Figure 5 shows the best fit of the model (dotted line) to the supercritical part of the measured height profile with $q = 10.0 \text{ cm}^2 \text{ s}^{-1}$. This fit and similar fits of the other measured height profiles in the 0.8 cm channel gave the average $\kappa = 0.07$. For the 0.4 cm channel, we obtained $\kappa = 0.07$ and for the 1.2 cm channel we found $\kappa = 0.06$. We thus find that the slopes of the measured height profiles decrease slightly when the channel width is increased. The corresponding eddy viscosities are up to an order of magnitude larger than the kinematic viscosity of water. We note that for a boundary layer on a flat plate without a free surface, a typical choice is $l_m \approx 0.09\delta$ as described by White (2006).

Watson (1964) presents a more elaborate approximate theory for the supercritical regime of turbulent channel flow. He assumes an eddy viscosity varying through the

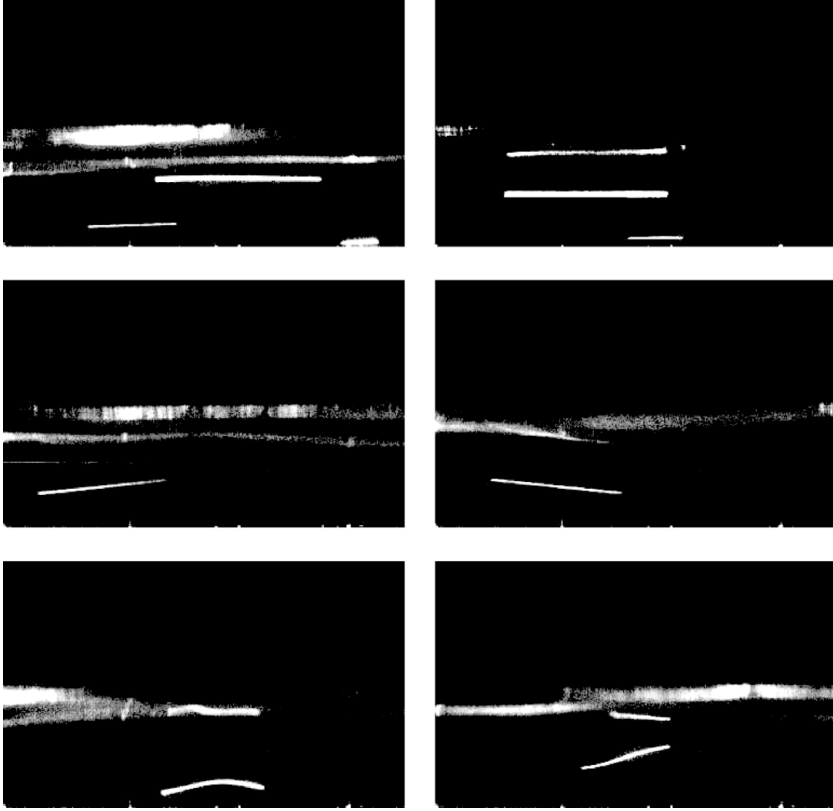


FIGURE 6. Six snapshots of particle tracks visualizing the turbulence in the supercritical region in the 0.8 cm channel with $q = 10.2 \text{ cm}^2 \text{ s}^{-1}$. The field of view was $0.8 \text{ cm} \times 0.5 \text{ cm}$, and the area was located 4 cm upstream of the jump. We used neutrally buoyant spherical tracer particles with diameter of $100 \mu\text{m}$, and an exposure time of $4 \times 10^{-3} \text{ s}$. The particle tracks were obtained using a laser sheet in the mid-plane of the channel. We show the raw particle tracks, and therefore the intensities of the tracks vary according to their position in the laser sheet. The channel bottom coincides with the lower edges of the pictures, and the fluctuating free surface is visible as the blurred horizontal regions in the middle of the pictures.

layer as $v_\varepsilon \propto u^6$, so as to agree with the Blasius boundary-layer solution near the bottom. The similarity solution then has the form $h(x) = \text{constant} (v/q)^{1/4} (x - x_0)$. Although we cannot convincingly distinguish between our claim that the slope of h is independent of q and a very weak dependence like $q^{-1/4}$, we also cannot verify the more detailed assumptions made by Watson, nor the values of the constants given. Thus, we believe that our simplistic mixing-length approach is more appropriate, being based only on the characteristic length scale and thus also applicable to the subcritical regime.

In the one-dimensional hydraulic jump experiment by Singha, Bhattacharjee & Ray (2005) for flows at similar Reynolds numbers in a wide channel, the measured slope of the free-surface height before the jump was also an order of magnitude larger than the slope predicted by the laminar height profile (3.4), again suggesting that the flow is turbulent. Based on the measurements by Singha, Bhattacharjee & Ray (2005), we estimate the value of $\kappa \approx 0.08$, although we do not have sufficient information from

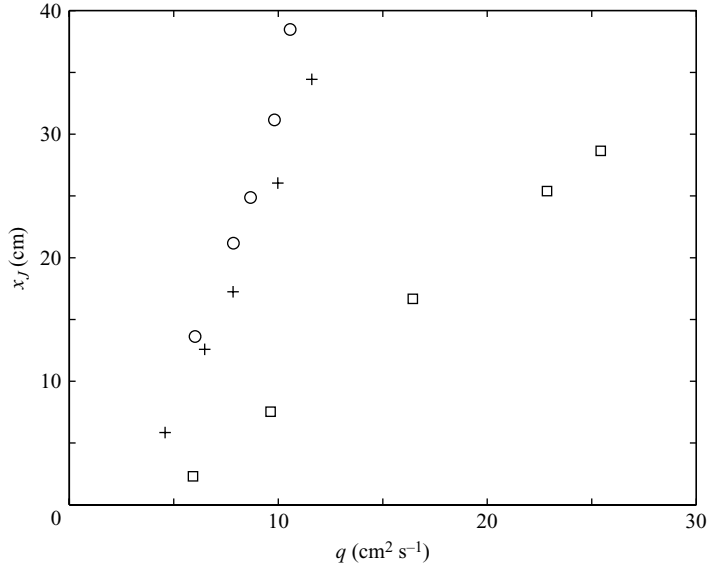


FIGURE 7. Measured jump position as a function of flow rate per unit transverse length for the three different channel widths 0.4 cm (□), 0.8 cm (+), and 1.2 cm (○).

the paper to test the dependence on flow rate, since measured surface heights are only presented for two different flow rates.

3.3. Jump position and effect of surface tension

The position of the hydraulic jump x_J moves downstream when q is increased as mentioned briefly in §3.1. Figure 7 shows x_J as a function of q for the three different channels. We notice that x_J increases faster with q as the channel width is increased, and we observe that x_J increases linearly with q in the $d = 0.4$ cm channel, whereas x_J increases faster than linearly with q in the channels with $d = 0.8$ cm and $d = 1.2$ cm. We speculate that these differences arise since the channel width for the 0.4 cm channel is smaller than the height of the fluid layer in the subcritical region by a factor of 2 to 4, whereas the channel width is comparable to the height of the fluid layer in the subcritical region in the two wider channels.

Our channel is designed primarily for intermediate flow rates, where capillarity plays a minor role. For the lowest flow rates this is, however, not true, and the precise shape of the outlet influences the height of the subcritical layer. We observe that in the limit of zero flow rate, a finite layer of fluid remains in the channel of height 0.2 – 0.4 cm, somewhat dependent on how the flow rate is decreased. The height of this layer is of the order of the capillary length $l_c = \sqrt{\sigma/g_0\rho}$, where σ is the surface tension and ρ is the density of the fluid. More precisely, the largest remaining heights are close to the maximal height of a large drop with a contact angle close to 90° , $\sqrt{2}l_c \approx 0.38$ cm in water. This means also that the position of the jump is slightly dependent on surface tension for the low flow rates. For larger flow rates, the influence of surface tension is negligible, as we verified by carrying out the channel experiment by adding surfactant in the form of sodium lauryl sulfate to the water. This should be contrasted with the circular hydraulic jump, where the radius of the jump is significantly influenced by capillarity owing to the curvature of the circle forming the jump (Bush & Aristoff 2003). In the channel experiment, the curvature of the free surface in a cross-section

takes both positive and negative values, and thus surface tension has no significant direct effect on the shape and location of the jump.

4. Averaging method for the entire flow

4.1. Averaged boundary-layer equation

For a description of the entire flow, we use the boundary-layer approximation and vertical averaging as the starting point. In the region downstream of the jump, the slowness of the flow and the large height of the fluid layer make the boundary-layer approximation doubtful. However, as in earlier work (Tani 1949; Watanabe, Putkaradze & Bohr 2003; Singha, Bhattacharjee & Ray 2005), we shall still use this approach and combine it with lateral averaging. In our case, the small separation between the channel walls introduces additional friction and the turbulence introduces an eddy viscosity, as discussed in § 3.2. The boundary-layer approximation for a time-independent and incompressible flow with a free surface of height h and hydrostatic pressure is

$$u \frac{\partial u}{\partial x} + w \frac{\partial u}{\partial z} = -g_0 \frac{\partial h}{\partial x} + \nu_\varepsilon \left(\frac{\partial^2 u}{\partial y^2} + \frac{\partial^2 u}{\partial z^2} \right), \quad (4.1)$$

together with the continuity equation

$$\frac{\partial u}{\partial x} + \frac{\partial w}{\partial z} = 0, \quad (4.2)$$

and mass conservation

$$q = \int_0^h dz \int_0^d dy u(x, y, z), \quad (4.3)$$

where u and w are the horizontal and vertical velocity components, respectively, and y is in the lateral direction spanning the space between the walls (see the coordinate system in figure 1). We assume that there is no flow in the lateral direction, and we neglect the dependence of the height of the fluid layer on the lateral direction. At the solid surfaces, we assume no-slip, and on the free surface, we approximate the boundary condition by

$$\left. \frac{\partial u}{\partial z} \right|_{z=h(x)} = 0. \quad (4.4)$$

To simplify the model, we shall now average in the y -direction and in the z -direction, and we shall assume that the velocity profile is separable and self-similar, i.e. that it can be written $u(x, y, z) = v(x)g(y/d)f(z/h(x))$, where $\int_0^1 g(\xi)d\xi = \int_0^1 f(\eta)d\eta = 1$. By the continuity equation, u and w must have the same y -dependence $g(y/d)$, and we obtain by averaging in the y -direction

$$G \left(u \frac{\partial u}{\partial x} + w \frac{\partial u}{\partial z} \right) = -g_0 \frac{dh}{dx} - \nu_\varepsilon \left(\frac{eu}{d^2} - \frac{\partial^2 u}{\partial z^2} \right), \quad (4.5)$$

where $G = \int_0^1 g^2(\xi) d\xi$, u and w are now the averages over y and $e = -2g'(1)$. For a parabolic profile $g(\xi) = 6\xi(1-\xi)$, we obtain $e = 12$ and $G = 6/5$. We now integrate the horizontal momentum equation (4.5) with respect to z from 0 to $h(x)$ and use the

continuity equation and the surface boundary condition (4.4) to obtain the averaged momentum equation

$$G \frac{1}{h} \frac{d}{dx} \left[\int_0^h u^2 dz \right] = -g_0 \frac{dh}{dx} - v_\varepsilon \left(\frac{ev}{d^2} + \frac{1}{h} u_z|_{z=0} \right), \quad (4.6)$$

which, using mass conservation, can be written as

$$G v(F v)' = -g_0 h' - v_\varepsilon \left(\frac{ev}{d^2} + \frac{1}{h} u_z|_{z=0} \right), \quad (4.7)$$

where $F = \int_0^1 f^2(\eta) d\eta$. We follow Watanabe *et al.* (2003) and assume a cubic velocity profile $u(x, z) = v(x)(a\eta + b\eta^2 + c\eta^3)$, where $\eta = z/h(x)$ and a, b and c are functions of x . To satisfy the no-slip condition, $u(x, 0) = 0$, we exclude the possibility of a constant term in the velocity profile. The three parameters can be expressed in terms of a single shape parameter λ as $a = \lambda + 3$, $b = -(5\lambda + 3)/2$ and $c = 4\lambda/3$. These relations follow from the absence of shear stress on the free surface (4.4) and mass conservation. With the cubic velocity profile we find

$$F(\lambda) = \frac{6}{5} - \frac{\lambda}{15} + \frac{\lambda^2}{105}, \quad (4.8)$$

and

$$u_z|_{z=0} = \frac{(3 + \lambda)v}{h}. \quad (4.9)$$

For comparison with the measured height profiles we will use a constant value of λ , but as we discuss in §4.4, it is necessary to allow λ to vary with x to model the flow in the jump region. For constant λ , we can write the governing equation as

$$q^2 G F(\lambda) \frac{h'}{h^3} = g_0 h' + v_\varepsilon \left(\frac{eq}{hd^2} + \frac{(3 + \lambda)q}{h^3} \right). \quad (4.10)$$

We now rescale the equation in units of the critical height $h_c = (GF)^{1/3} q^{2/3} g_0^{-1/3}$. Using the rescaling, we obtain $h = h_c H = (GF)^{1/3} q^{2/3} g_0^{-1/3} H$, $x = (GFq/v_\varepsilon) h_c X = (GF)^{4/3} v_\varepsilon^{-1} q^{5/3} g_0^{-1/3} X$ and $e_s = (h_c/d)^2 e = (GF)^{2/3} q^{4/3} g_0^{-2/3} d^{-2} e$. For fixed λ , the averaged boundary-layer equation in rescaled variables thus takes the form

$$(1 - H^3) \frac{dH}{dX} = A + e_s H^2, \quad (4.11)$$

where $h = (GF)^{1/3} q^{2/3} g_0^{-1/3} H$, $x = (GF)^{4/3} v_\varepsilon^{-1} q^{5/3} g_0^{-1/3} X$ and $A = 3 + \lambda$. We note that our definition of the critical height h_c is different from the conventional definition by the numerical factor $(GF)^{1/3}$. In the following, we show how to use (4.11) to model supercritical and (with slight modification) subcritical channel flows, and we compare numerical solutions of the averaged equation with the measured height profiles.

4.2. Modelling the channel flows

In the supercritical region we shall assume that the vertical velocity profile is close to the solution by Watson (1964), which is not far from parabolic ($\lambda = 0$). The laminar solution by Watson has $F \approx 1.26$ and $f'(0) = 2.28$. In the variable λ approach (see §4.4) we in fact obtain $\lambda \approx -3/5$ with $F(\lambda = -3/5) \approx 1.24$ and $f'(0) = 3 + \lambda = 2.4$

for the supercritical flow. Since in this regime, h is the smallest length scale, we shall also assume that the viscosity is given by the eddy viscosity (3.5), i.e. $\nu_\varepsilon \approx \kappa^2 q$, which changes the rescaling to $x = \kappa^{-2}(GF)^{4/3}q^{2/3}g_0^{-1/3}X = \kappa^{-2}GFh_cX$, so we shall write

$$(1 - H^3)\frac{dH}{dX} = A + e_s H^2, \quad (4.12)$$

with

$$x = \kappa^{-2}GFh_cX, \quad (4.13)$$

where $A = 2.28$. The upstream boundary condition for the flow is $H(X_0) = 0$ at $X = X_0$. The measured height profiles shown in figure 4 extrapolate to zero somewhere before the nozzle, and the point X_0 was different for the different channel widths, since the nozzles and the nozzle heights above the channel bottom were different in the three set-ups.

In the subcritical region, h is typically larger than d , and we shall assume that the mixing length now becomes proportional to d and not to h , i.e. $l_m = \kappa_y d$. Then $\nu_\varepsilon \approx l_m^2 |\partial u / \partial y| \approx l_m^2 u / d = \kappa_y^2 d u = \kappa_y^2 d q / h$. If $\kappa_y = \kappa$ (which we assume in the following), we find $\nu_\varepsilon^{outer} \approx (d/h)\nu_\varepsilon^{inner}$, which even for the narrow 0.4 cm channel remains of a size similar to the eddy viscosity $\nu_\varepsilon^{inner} = \kappa^2 q$. Thus, the rescaled boundary-layer equation in the subcritical region becomes

$$(1 - H^3)\frac{dH}{dX} = \frac{1}{H}(A + e_s H^2), \quad (4.14)$$

now with

$$x = \kappa^{-2}(GF)^{4/3}q^{4/3}g_0^{-2/3}d^{-1}X = \kappa^{-2}GF(h_c/d)h_cX, \quad (4.15)$$

and assuming in this case simply a parabolic velocity profile $A = 3$. Again, as above, we might obtain other factors when averaging powers of u coming from the eddy viscosity, but this will in effect only change the value of κ .

The equations (4.12) and (4.14) can be solved exactly for the inverse function $X(H)$. Letting $Y = AX$ and $a = e_s/A$, the solution of (4.12) is

$$Y(H) = -\frac{1}{2}a^{-1}H^2 + a^{-1/2} \tan^{-1}(a^{1/2}H) + \frac{1}{2}a^{-2} \log(1 + aH^2) + C, \quad (4.16)$$

which in the limit $a \rightarrow 0$ gives $Y(H) = H - H^4/4$ (Singha *et al.* 2005). For (4.14), the solution is

$$Y(H) = a^{-2}H - \frac{1}{3}a^{-1}H^3 - a^{5/2} \tan^{-1}(a^{1/2}H) + \frac{1}{2}a^{-1} \log(1 + aH^2) + C. \quad (4.17)$$

In both cases, the solutions have a single maximum in the physical regime where both X and H are positive: since the derivative $X'(H)$ has the sign of $1 - H^3$, it is increasing (with $C = 0$) for $0 < H < 1$ and decreasing for $1 < H < H_f$, where $X(H_f) = 0$, see figure 8(a). The inverse functions $H(X)$ are multiple valued, see figure 8(b), but if we want to interpret the upper branch of (4.16) as a subcritical solution, we have to use different values of the constant C in the two regions: for $C = 0$ (or near zero) the lower branch of $H(X)$ from (4.16) describes the supercritical state. For the subcritical state outside the jump, the boundary condition must be set at the outlet (say $X = L$) where the height must be critical ($H = 1$). This means that the upper branch of $H(X)$ from (4.16) must be translated to the right to fit this condition and the location of the jump is then determined by a shock condition (here, the Rayleigh condition as

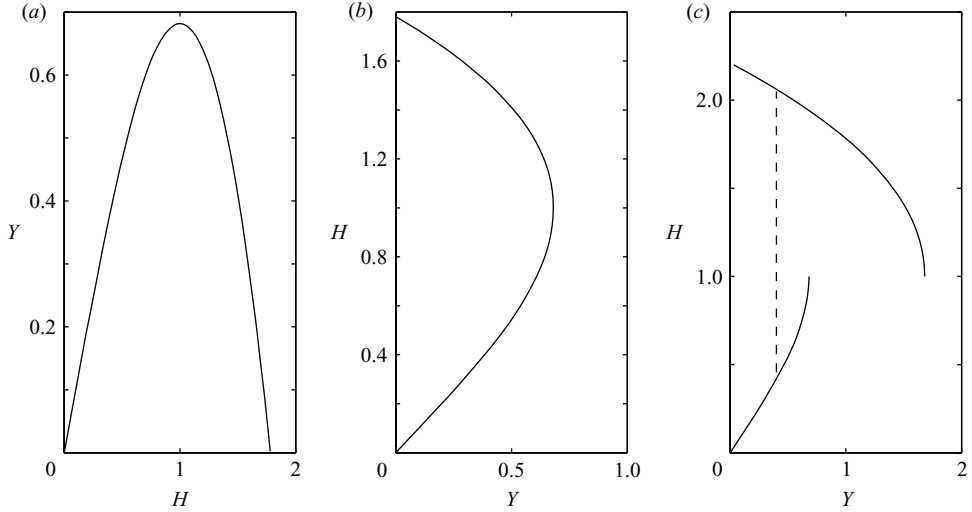


FIGURE 8. Structure of the solutions of the averaged boundary-layer equations (4.12) and (4.14). (a) Implicit solution $Y(H)$ of (4.12) as given by (4.16) with $C=0$ and $a=0.5$. (b) Solution $H(Y)$ obtained by interchanging the axes. (c) Solution with a discontinuity (shock) obtained by translating the upper part of (b) to satisfy the critical condition ($H=1$) at the outlet. This means that in this regime we choose a different integration constant, here $C=1$. The location of the jump (dashed line) is found from the jump condition (4.20). The structure of the solutions is similar for flows without sidewalls, i.e. $a=e_s=0$.

discussed in the next section). Figure 8(c) shows the general structure of the solutions obtained in this way. In our comparison to the experiments we shall use (4.16) for the supercritical solution and (4.17) for the subcritical solution, but qualitatively the structure is similar.

Figure 9 shows that there is good overall agreement between the solutions of the averaged boundary-layer equations (4.12) and (4.14) and the measured height profile with $q=10.0\text{ cm}^2\text{ s}^{-1}$. The height profile in the supercritical region curves slightly upward in the model owing to friction from the sidewalls, an effect which is not accounted for in the two-dimensional solution by Watson (1964). The precise modelling is complicated at the outlet where the flow exits the channel. As in earlier work (Bohr *et al.* 1993; Singha *et al.* 2005), we simply assume that the critical height $H=1$ is reached slightly beyond the outlet. This works well for $q=10.0\text{ cm}^2\text{ s}^{-1}$ as shown in figure 9, but the solution of equation (4.14) underestimates the measured surface height in the subcritical region for low flow rates as shown by the dotted curve for $q=4.6\text{ cm}^2\text{ s}^{-1}$ in figure 10. The solid line is the solution obtained by adjusting the value of the outlet height, and we see that this gives a good fit to the data. The discrepancy in the outlet height is connected with a fact mentioned in §3.3: that capillarity strongly influences the outflow at low flow rates, leaving a finite layer of fluid in the channel even for the smallest flow rates. Thus it will be impossible to obtain an outlet height smaller than the height of that layer (of the order of the capillary length) – at least with our outlet condition.

4.3. Jump condition

Both the inner and outer equations diverge at the critical height $H=1$, and thus we cannot integrate them across the jump. Instead, we assume that a shock occurs, and that the flow rate and the average momentum are conserved across the discontinuity.

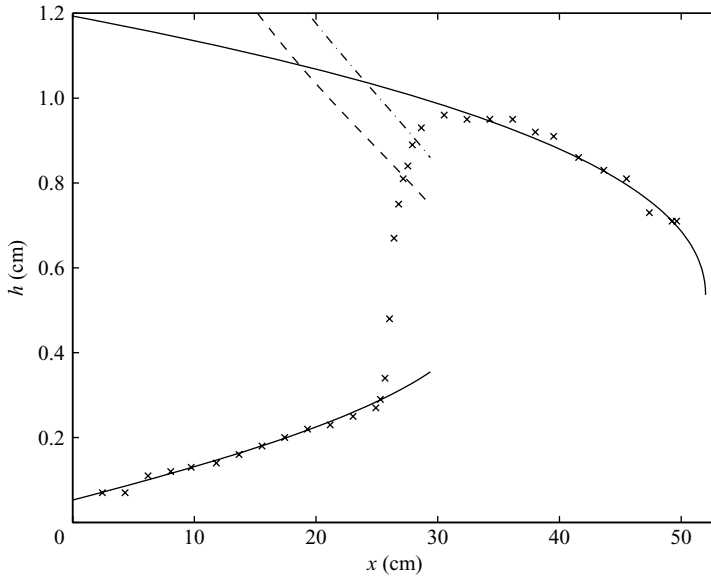


FIGURE 9. Measured height profile (\times) and theoretical height profiles in the supercritical and in the subcritical flow region (solid curves) for the flow in the 0.8 cm channel with $q = 10.0 \text{ cm}^2\text{s}^{-1}$. For both theoretical curves we used $\kappa = 0.065$. The dashed curve and the dash-dot curve show the height to which the supercritical flow is expected to jump based on the Rayleigh jump condition (4.21) with two different values of GF as discussed in the text.

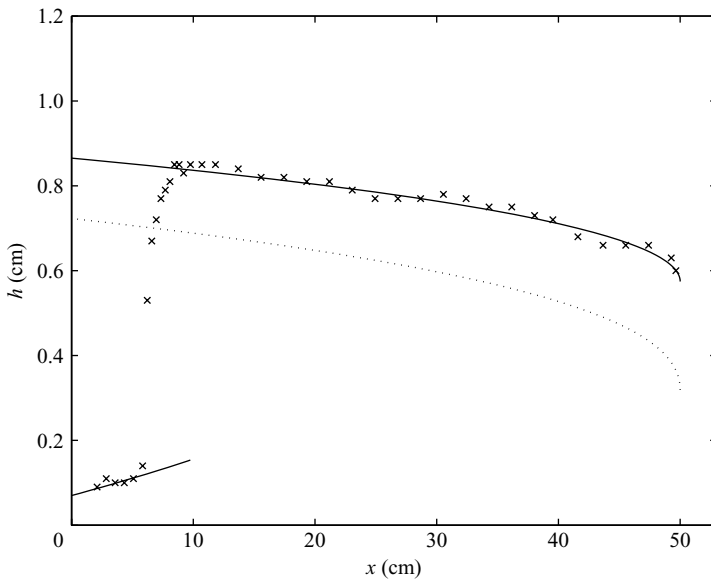


FIGURE 10. Measured height profile (\times) and theoretical height profile in the supercritical flow region (solid curve) for the flow in the 0.8 cm channel with $q = 4.6 \text{ cm}^2\text{s}^{-1}$. Two theoretical curves are shown in the subcritical flow region, one with an outer ‘critical height’ of 1.8 times the one used before the jump (solid curve) and one with the same critical height as before the jump (dotted curve). For all three theoretical curves we used $\kappa = 0.065$.

Following the standard procedure introduced by Rayleigh (1914), we find

$$\begin{aligned} \frac{1}{\rho} \int_0^d dy \int_0^{h_1} dz p_1(y, z) + \int_0^d dy \int_0^{h_1} dz u_1^2(y, z) \\ = \frac{1}{\rho} \int_0^d dy \int_0^{h_2} dz p_2(y, z) + \int_0^d dy \int_0^{h_2} dz u_2^2(y, z), \end{aligned} \quad (4.18)$$

where h_1 and h_2 are the heights of the fluid layer immediately before and after the jump, respectively, as shown in figure 1. With hydrostatic pressure we obtain the equation

$$\frac{1}{2} g_0 h_1^2 + GF h_1 v_1^2 = \frac{1}{2} g_0 h_2^2 + GF h_2 v_2^2, \quad (4.19)$$

and using mass conservation, $q = h_1 v_1 = h_2 v_2$, we can rewrite this as

$$\frac{1}{2} g_0 h_1^2 + GF \frac{q^2}{h_1} = \frac{1}{2} g_0 h_2^2 + GF \frac{q^2}{h_2}. \quad (4.20)$$

Here, we have for simplicity assumed that the profiles before and after the jump are similar. This is of course not precisely true, but with the lack of more precise information, this seems a reasonable choice. The non-trivial solution of the cubic equation is

$$h_2 = \frac{1}{2} h_1 \left(\sqrt{1 + 8Fr_e^2} - 1 \right), \quad (4.21)$$

where the effective Froude number immediately before the jump is

$$Fr_e = \frac{\sqrt{GF} q}{g_0^{1/2} h_1^{3/2}}. \quad (4.22)$$

The dashed curve and the dash-dot curve in figure 9 show the heights to which the supercritical flow is expected to jump, based on the Rayleigh jump condition (4.21) with two different effective Froude numbers, and the intersections between the two curves and the solid curve showing the solution of (4.14) therefore give theoretical predictions of the jump position. The velocity profile after the jump, which is required for an accurate determination of the momentum flux, is not known precisely, and we therefore assume either that the velocity profiles before and after the jump are both close to the solution by Watson (dashed) or that the velocity profiles have a somewhat larger effective flow rate with $\sqrt{GF} = 1.35$ (dash-dot). The prediction with $\sqrt{GF} = 1.35$ agrees well with the measurements, whereas the model using the Watson profile predicts that the jump position should be approximately 5 cm further upstream than observed experimentally. We speculate that the difficulty in determining the jump location accurately is due to our lack of knowledge about the precise flow structure after the jump. We discuss the flow structure and the averaging model further in the next section.

4.4. Flow structure in the jump region

As has been shown earlier (Bohr, Putkaradze & Watanabe 1997; Watanabe *et al.* 2003) for the radial hydraulic jump and for flow down an inclined plane, it is possible to compute the flow structure through the jump using the averaging method if the shape parameter λ is allowed to vary with x . The same method can be applied to the present case of a hydraulic jump in a horizontal channel starting with (4.7) and the eddy viscosity (3.5). The inclusion of a shape parameter means that an additional

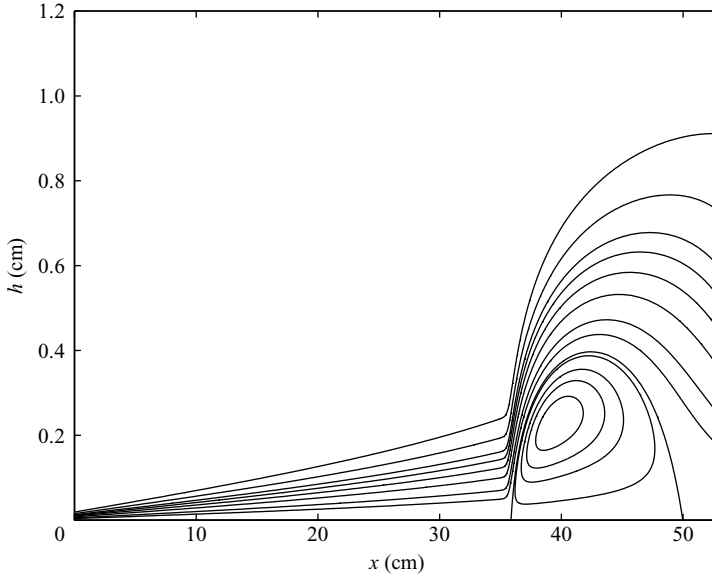


FIGURE 11. Streamline pattern obtained by solving the two averaged equations (4.23) through the jump region. The parameter values were the same as in figure 9. The uppermost streamline coincides with the free surface. Notice the large separation zone after the hydraulic jump.

equation is required in addition to the average momentum equation. As in earlier work, we take this as the y -averaged momentum equation evaluated at $z=0$ and obtain the equations:

$$\lambda' = \frac{1}{F'(\lambda)} \left(\frac{4\lambda}{H} - F(\lambda) \frac{5\lambda + 3}{H^4} - e_s H \right), \quad H' = -\frac{5\lambda + 3}{H^3}. \quad (4.23)$$

As shown in figure 11, we do find solutions going through the jump, where an inner branch, closely reminiscent of the Watson solution (with $\lambda \approx -3/5$), makes a continuous, but rapid transition to a subcritical state with $\lambda \approx 0$. Continuing to the right the solution will diverge as expected when the critical condition is met.

In the jump region, the solution has a large separation zone. Hydraulic jumps in thin layers typically show separation, so this is to be expected. However, our flow is turbulent and this is modelled only by taking into account an eddy viscosity. Experimentally, we do not see clear signs of an ordered mean flow in the form of a separation vortex. The height profile through the jump is also not very well represented by (4.23). Comparing with the experimental profiles in figure 4, it is clear that the width of the jump region is overestimated – again presumably due to the simplistic turbulence modelling.

5. Sheet experiment with rhombic jump region

Figure 3 shows the surprising result that the hydraulic jump takes the form of a rhombus in the sheet experiment. When we change the flow rate, Q , it is the opening angle of the rhombus, θ , that changes, reminiscent of the classical Landau–Levich problem in which a solid plate is withdrawn from a liquid bath (Blake & Ruschak 1979) or the Mach cone formed behind a supersonic projectile (Faber 1995). Our key observation is that the opening angle (see schematic illustration in figure 12(a))

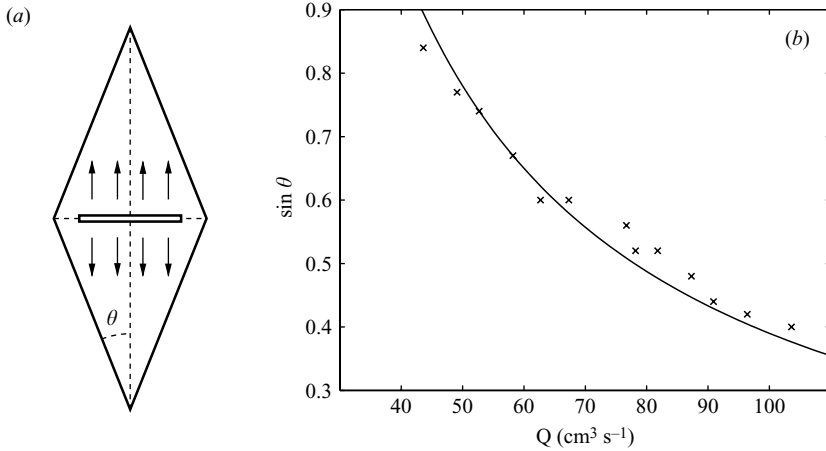


FIGURE 12. (a) Schematic illustration of the sheet experiment and definition of the opening angle, θ , of the rhombic jump region. (b) Sine of θ as function of the flow rate, Q . The measurements (\times) are compared with the inverse proportionality expected for a constant normal velocity at the hydraulic jump (solid line).

for definition) is determined by the condition that the fluid velocity normal to the boundary immediately before the jump is constant. The value of the normal velocity follows directly from measurements of the flow rate and of the height of the fluid layer in the interior of the jump region. The height measurements show that the thickness within the thin film region is constant to within the experimental accuracy – about 0.01 cm. This is to be expected for this experiment, since the lack of confining walls should lead to a flow that remains laminar, and indeed we were not able to detect any turbulence in the experiment, contrary to what we found in the channel experiment.

Figure 12(b) shows measurements of the opening angle, θ , of the rhombus as a function of the flow rate, Q . The measurements are compared with the prediction obtained by assuming that the normal velocity at the jump is constant and equal to $29 \pm 6 \text{ cm s}^{-1}$. The rhombic shape of the jump region is typical of ‘oblique standing waves’ (Ippen & Harleman 1956), which are completely analogous to oblique shock waves in gases, and typically occur in channel flows because of a sudden contraction of the width. In the shock approximation (Chow 1959; Ippen & Harleman 1956; Liepmann & Roshko 1957), the normal velocity jumps, whereas the velocity parallel to the shock is unchanged. Thus, the jump condition becomes

$$h_2 = \frac{1}{2}h_1 \left(\sqrt{1 + 8Fr_1^2 \sin^2 \theta} - 1 \right), \quad (5.1)$$

where $Fr_1 = v_1 / \sqrt{g_0 h_1}$ is the Froude number before the jump. Thus, the constancy of the inner height h_1 and the normal velocity implies that $Fr_1 \sin \theta$ is constant and therefore that h_2 is constant. We believe that the constancy of h_2 is related to capillary effects, as for the low flow rates in the channel. Indeed, the height of the outer layer is approximately $h_2 = 0.35 \text{ cm}$, again close to $\sqrt{2}l_c = 0.38 \text{ cm}$.

6. Conclusion

We have studied two realizations of one-dimensional hydraulic jumps. In both cases, our results are consistent with the treatment of the flow in terms of a shock

connecting a supercritical and a subcritical flow. In the sheet case, the shock becomes oblique and the jump occurs at a constant normal velocity. In the narrow channel, the flow is turbulent, and the slope of the linearly increasing height profile upstream of the jump is strongly enhanced in comparison with the laminar-flow situation. A simple mixing-length model of the turbulence reproduces the experimental results, and an averaged boundary-layer model describes the flow both upstream and downstream of the jump.

T. B. is grateful for the warm hospitality at the Laboratoire de Physique Statistique, Ecole Normale Supérieure, Paris while this work was initiated. We thank Erik Hansen for his careful construction of the channel experiment.

REFERENCES

- BLAKE, T. D. & RUSCHAK, K. J. 1979 A maximum speed of wetting. *Nature* **282**, 489–491.
- BOHR, T., DIMON, P. & PUTKARADZE, V. 1993 Shallow-water approach to the circular hydraulic jump. *J. Fluid Mech.* **254**, 635–648.
- BOHR, T., PUTKARADZE, V. & WATANABE, S. 1997 Averaging theory for the structure of hydraulic jumps and separation in laminar free-surface flows. *Phys. Rev. Lett.* **79**, 1038–1041.
- BUSH, J. W. M. & ARISTOFF, J. M. 2003 The influence of surface tension on the circular hydraulic jump. *J. Fluid Mech.* **489**, 229–238.
- CHOW, V. T. 1959 *Open Channel Hydraulics*. McGraw–Hill.
- DEFINA, A. & SUSIN, F. M. 2003 Stability of a stationary hydraulic jump in an upward sloping channel. *Phys. Fluids* **15**, 3883–3885.
- FABER, T. E. 1995 *Fluid Dynamics for Physicists*. Cambridge University Press.
- HIGUERA, F. J. 1994 The hydraulic jump in a viscous laminar flow. *J. Fluid Mech.* **274**, 69–92.
- HOLLAND, D. M., ROSALES, R. R., STEFANICA, D. & TABAK, E. G. 2002 Internal hydraulic jumps and mixing in two-layer flows. *J. Fluid Mech.* **470**, 63–83.
- HORNUNG, H. G., WILLERT, C. & TURNER, S. 1995 The flow downstream of a hydraulic jump. *J. Fluid Mech.* **287**, 299–316.
- IPPEN, A. T. & HARLEMAN, D. R. F. 1956 Verification of theory for oblique standing waves. *Trans. ASCE* **121**, 678–694.
- LIEPMANN, H. W. & ROSHKO, A. 1957 *Elements of Gas Dynamics*. Wiley.
- OLSSON, R. G. & TURKDOGAN, E. T. 1966 Radial spread of a liquid stream on a horizontal plate. *Nature* **211**, 813–816.
- POPE, S. B. 2000 *Turbulent Flows*. Cambridge University Press.
- RAYLEIGH, LORD 1914 On the theory of long waves and bores. *Proc. R. Soc. Lond. A* **90**, 324–328.
- RUSCHAK, K. J., WEINSTEIN, S. J. & NG, K. 2001 Developing film flow on an inclined plane with a critical point. *ASME J. Fluids Engng* **123**, 698–702.
- SIMPSON, J. E. 1997 *Gravity Currents: In the Environment and the Laboratory*, 2nd Edn. Cambridge University Press.
- SINGHA, S. B., BHATTACHARJEE, J. K. & RAY, A. K. 2005 Hydraulic jump in one-dimensional flow. *Eur. Phys. J. B* **48**, 417–426.
- SVENDSEN, I. A., VEERAMONY, J., BAKUNIN, J. & KIRBY, J. T. 2000 The flow in weak turbulent hydraulic jumps. *J. Fluid Mech.* **418**, 25–57.
- TANI, I. 1949 Water jump in the boundary layer. *J. Phys. Soc. Japan* **4**, 212–215.
- WATANABE, S., PUTKARADZE, V. & BOHR, T. 2003 Integral methods for shallow free-surface flows with separation. *J. Fluid Mech.* **480**, 233–265.
- WATSON, E. J. 1964 The radial spread of a liquid jet over a horizontal plane. *J. Fluid Mech.* **20**, 481–499.
- WHITE, F. M. 2006 *Viscous Fluid Flow*. McGraw–Hill.